

# Quantitative AFM analysis of phase separated borosilicate glass surfaces

D. Dalmas\*, A. Lelarge and D. Vandembroucq

*Laboratoire "Surface du Verre et Interfaces"  
Unité Mixte CNRS/Saint-Gobain  
39 Quai Lucien Lefranc, 93303 Aubervilliers, France*

---

## Abstract

Phase separated borosilicate glass samples were prepared by applying various heat treatments. Using selective chemical etching we performed AFM measurement on the phase separated glass surfaces. A quantitative roughness analysis allowed us to measure precisely the dependence of the characteristic size of the phase domains on heating time and temperature. The experimental measurements are very well described by the theoretically expected scaling laws. Interdiffusion coefficients and activation energy are estimated from this analysis and are consistent with literature data.

*Key words:* Atomic force microscopy, phase separation, borosilicates, morphology, correlation function

*PACS:* 68.37.Ps, 61.43.Fs, 64.75.+g

---

## 1 Introduction

Within the last 20 years Atomic Force Microscopy (AFM) has become a standard tool in glass science[1]. Beyond the direct roughness measurements, AFM has been applied to study the glass structure, corrosion, fracture, polishing and progressively more to characterize various (organic or inorganic) coatings deposited on glasses. Increasingly precise measurements have been obtained in the last years allowing to reach atomic resolution [2,3]. Apart from detailed studies of the scale invariant character of the roughness of fracture surfaces[4] or the recent description of fused glass surfaces in terms of frozen capillary

---

\* corresponding author

*Email address:* davy.dalmas@saint-gobain.com (D. Dalmas).

waves[5], AFM roughness analysis is often restricted to the simple determination of the standard deviation of the height fluctuations, *i.e.* the RMS roughness. This RMS roughness indicator which only gives information on the out of plane surface fluctuations is however a rather poor information as compared to the available information in the entire image. The characterization of in-plane features, *e.g.* the typical size of patterns on the surface requires the use of the height auto-correlation function.

In this paper we develop a quantitative analysis of AFM roughness data to study the kinetics of phase separation coarsening stage in glasses. AFM measurement has been used to study phase separation but mostly to image the surface of thin polymer films [6,7,8,9,10,11]. The development of phase separation in glasses has been intensively studied experimentally in the last decades[12]. Various techniques have been used to follow this phenomenon : visible or X scattering[13,14,15,16,17], electronic microscopy[18,19], infrared or Raman spectroscopy[20,21,22,23]... Most of the times, these techniques are used to test the occurrence of phase separation and to describe its morphology (droplet or interconnected). Few studies (generally based on electronic microscopy or X-ray scattering) give a quantitative estimate of the volume fraction of the two separated phases and sometimes of the typical size of the domains. X-ray and visible light scattering techniques have been intensively used to characterize the kinetics of phase separation, from the early stage of binodal or spinodal phase decomposition up to the scaling behavior of the coarsening stage[12]. More recently, coherent X-ray techniques have been used to probe the dynamics of fluctuations during domain coarsening of a sodium borosilicate glass[24].

In the present work we focus our study on a sodium-potassium borosilicate glass. Alkali borosilicate glasses[12] are known for their large composition domain allowing phase separation. After heat treatment and etching we perform AFM surface measurements in order to reveal the internal structure. The paper is organized as follows. We first describe the experimental methods: melting, sample preparation, heat treatments, chemical etching and AFM measurements. We then present the topographic results obtained by AFM, giving a special attention to the statistical analysis. We finally compare our results with theoretical descriptions for phase separation kinetics and we extract estimates of interdiffusion coefficient and activation energy.

## 2 Experimental

### 2.1 Material

A sodium potassium borosilicate glass of weight composition  $\text{SiO}_2$  70%,  $\text{B}_2\text{O}_3$  25%,  $\text{Na}_2\text{O}$  2.5% and  $\text{K}_2\text{O}$  2.5% has been prepared as follows: i) The raw materials are mixed and melted at  $1550^\circ\text{C}$  in a  $800\text{ cm}^3$  platinum crucible; ii) The glass is then refined during 2 hours in order to obtain an homogeneous glass; iii) After quenching, glass is rapidly transferred to an electric furnace to be annealed during 1h at  $630^\circ\text{C}$ , in order to relax the internal thermal stresses; iv) The glass is finally cooled to room temperature by opening the furnace door. After preparation, a cylindrical sample is core drilled and then cut into centimeter thick slices. At that stage, the glass is no longer transparent. Its opalescence is a signature of phase separation taking place over length scales comparable to the wavelengths of visible light. The major phase is expected to have a concentration close to pure silica while the minor phase concentrates the other constituents[12].

### 2.2 Thermal treatments

Two types of thermal treatments have been performed. Four thick slices are first submitted to a thermal treatment at  $650^\circ\text{C}$  of duration 1h, 4h, 16h and 64h respectively. Square samples of 0.5mm thickness are cut from the slices and then mechanically polished to obtain mirror smooth surfaces. Following this first method, the result of bulk phase separation can be observed at the surface. A second sample preparation has consisted of inverting the sequence: first cutting the square samples from a glass slice, polishing them and only then performing the thermal treatments. Following this second method, we can observe the influence of a surface on phase separation. Two series of thermal treatments have been performed, one at  $650^\circ\text{C}$  with seven different durations (1h, 2h, 4h, 8h, 16h, 32h, 64h and 96h) and a second one at six different temperatures ( $625^\circ\text{C}$ ,  $650^\circ\text{C}$ ,  $660^\circ\text{C}$ ,  $670^\circ\text{C}$ ,  $675^\circ\text{C}$  and  $680^\circ\text{C}$ ) during 16h. The first series allows us to study the influence of thermal treatment duration on phase separation morphology. The second one allows investigation of the influence of temperature. In all cases, the samples are heat-treated in an electric furnace and cooled to room temperature outside the furnace.

### 2.3 Etching

A selective attack with a slightly acid treatment ( $pH \approx 5$ ) is performed. The borate rich phase is thus eliminated in surface due to its very low chemical durability while the silica rich phase remains almost unaffected. The residual surface roughness then makes it possible to reveal the phase separation morphology as the composition contrast induces a height contrast. The alkali borate rich phase is thus expected to appear as depressions compared to the almost unmodified mirror surface corresponding to the silica rich phase.

### 2.4 AFM measurements

The surface morphology of all samples have been characterized by AFM height measurement in tapping mode (TM-AFM), using a Nanoscope III A from Digital Instruments with Al coated tip (BudgetSensors - model BS-Tap 300 Al). The Al coating thickness is 30nm, the resonant frequency is 300 kHz and the stiffness constant is 40N/m. The images have been recorded at a scan frequency between 0.8 and 1Hz for a resolution of  $512 \times 512$  pixels. For each samples (i.e. for each thermal treatment conditions), we perform at least 6 AFM images with 3 different scan areas. Depending on the size of the phase separation domains, the scan areas used are  $1 \times 1\mu m^2$ ,  $2 \times 2\mu m^2$ ,  $4 \times 4\mu m^2$  and  $8 \times 8\mu m^2$ .

## 3 Results

### 3.1 Morphology of phase separation domains

For all samples (cf. Fig. 1 and Fig. 2), we observed an interconnected morphology. On all these images, the grey scale is encoded such that the silica rich phase appears in clear colors and the borate rich phase appears in dark colors. On Fig. 1 (respectively on Fig. 2), one can easily see the influence of time (resp. temperature) of thermal treatment on the morphology: at a given temperature (resp. time), the characteristic size of spinodal phase separation domains increases with annealing time (resp. temperature).

As clearly shown on Fig. 3, we obtained patterns exhibiting a striking self-similar character. In particular with a well chosen set of thermal treatment duration and AFM image size, we obtain almost indistinguishable images. This self similar character simply reflects that space and time can be rescaled

altogether. We show below that AFM measurements allow us to go beyond this qualitative picture. In particular we will evidence that the kinetics of the phase domains obeys the expected scaling law  $\xi \propto t^{1/3}$  between the characteristic size  $\xi$  and the duration  $t$  of the thermal treatment (at a given temperature) in the coarsening stage of the phase separation process[12].

### 3.2 Statistical analysis of AFM images

In the following we use AFM measurements on etched surfaces to estimate the characteristic size of the phase separated domains. AFM measurements give an immediate access to the height field. To get information on the growth of the phase domains we will exploit the height autocorrelation function.

#### 3.2.1 Determination of the radial-mean auto-correlation function

In order to evaluate the characteristic length of phase separation domains for all our samples, we first calculate for all TM-AFM height images the normalized auto-correlation function  $C(\vec{R})$ , given by the following equation:

$$C(\vec{R}) = \frac{\langle h(\vec{x}) \cdot h(\vec{x} + \vec{R}) \rangle_{\vec{x}}}{\langle h(\vec{x}) \cdot h(\vec{x}) \rangle_{\vec{x}}} \quad (1)$$

where  $h(\vec{x})$  is the height in nanometers at a point of coordinate  $\vec{x}(r, \theta)$  and with  $C(\vec{0}) = 1$ . On Fig 4, we give an example of the three dimensional representation of the center part ( $0.5 \times 0.5 \mu m^2$ ) of the auto-correlation function  $C(\vec{R})$  calculated from the height matrix extracted from an AFM height images ( $4 \times 4 \mu m^2$ ). On this particular 3D representation and also for all other images, we obtain results characteristic of an isotropic random distribution of domains: a central peak surrounded by a few circular rings, corresponding to oscillations of vanishing amplitude. The isotropic character of the fluctuations allows for the use of an average auto-correlation function dependent on the only distance:

$$g(r) = \langle C(r, \theta) \rangle_{\theta} \quad (2)$$

Fig. 5 shows the auto-correlation function for a heat treatment of 16h at 650°C performed on two series of samples where the heat treatment has been applied before or after cutting and polishing operations. The evolution of  $g(r)$  as a function of the duration of heat treatment at 650°C and respectively as a function of temperature for a 16h heat treatment is given on Fig. 6 and Fig. 7 respectively. On these two figures,  $g(r)$  corresponds to the mean value of the auto-correlation function of the six AFM images associated with one sample.

### 3.2.2 Determination of two correlation lengths

The second step of our analysis of AFM height data consists of extracting for each sample a characteristic length from auto correlation function  $g(r)$ . We discuss here two typical lengths, chosen for their physical meaning with respect to phase separation phenomena. The first one, called  $\xi_{0.5}$ , is the value of  $r$  at  $g(r) = 0.5$  ( $g(\xi_{0.5}) = 0.5$ ) and corresponds to the mean size of the phase separation domains. The second one, called  $\xi_{min}$ , is the value of  $r$  when  $g(r)$  reached its first minimum ( $g(\xi_{min}) = \min(g(r))$ ) and corresponds to the mean distance between two domains of different composition. The evolution of these characteristic lengths with heat treatment duration and temperature are summarized in tables 1 and 2 and displayed in Fig. 9 and Fig. 10 respectively. These results are discussed in next section in the light of theoretical predictions for the kinetics of the coarsening stage of phase separation in glasses.

## 4 Discussion

The process of phase separation in a spinodal region is usually divided into two stages. The first one corresponds to the phase decomposition into domains at the two limit concentrations. The second one is the coarsening process, corresponding to the progressive growth of the domains, driven by surface tension and limited by diffusion. During this coarsening regime, the structure remains statistically self-similar and the evolution of the morphology is entirely controlled by the growth of the characteristic length of the domains which is expected to follow the Lifshitz-Slyozov-Wagner scaling:

$$R \approx (Kt)^{1/3}, \quad K \approx \frac{\gamma D v}{kT}, \quad (3)$$

where, within the classical mean field theory of coarsening[12,25]  $\gamma$  is the interfacial tension,  $D$  the interdiffusion coefficient and  $v$  a molecular volume. This result applies in case of conservation of the order parameter. Following Huse[26], it can be recovered *via* a simple scaling argument. Let us consider an interface of radius of curvature  $R$  separating two domains with a volume concentration difference  $\Delta c$ . Under local equilibrium, the Laplace pressure  $\gamma/R$  balances the osmotic pressure  $\mu \Delta c$  (where  $\mu$  is the chemical potential) so that  $\mu \simeq \gamma/R \Delta c$ . Assuming that fluctuations of the chemical potential are of the same order of magnitude as the chemical potential itself we have  $\nabla \mu \simeq \gamma/R^2 \Delta c$ . The flux of particles can thus be written  $j = M c \nabla \mu$  where  $M = D/kT$  is the particle mobility. Mass conservation finally gives for the

domain growth law:

$$\frac{dR}{dt} = \frac{j}{c} = \frac{\gamma D}{R^2 \Delta c k T} \quad (4)$$

from which we recover directly the scaling law (3).

In the following we shall compare our experimental results within this framework. The different durations of heat treatments allow us to study the temporal scaling of the coarsening regime and beyond, to estimate the diffusion constant. In a similar way, data from different temperatures of heat treatment, combined with the Arrhenian scaling of the mobility,  $M = M_0 \exp(-E_{in}/kT)$  provides a rough estimate of the corresponding activation energy.

#### 4.1 *Effect of surface*

We summarize on Fig. 5 the height autocorrelation functions obtained after a heat treatment of 16 hours at 650°C. Two types of preparation were used. As described above, the heat treatment was applied either before (series A) or after (series B) cutting and polishing the samples. This allows to test the effect of a surface on the coarsening process. As shown on Fig. 5 the correlation functions obtained on the two series of samples are almost identical. The presence of a surface thus does not seem to influence the coarsening and surface measurements can be considered as representative of the bulk morphology. The results presented in the following have been obtained by statistical averaging over the entire set of samples.

#### 4.2 *Effect of annealing time*

Let us note first that all samples described here were submitted to a primary annealing thermal treatment of 1h at 630°C. The latter is intended to relax thermal stresses but also induces phase separation in the present case. Additional thermal treatments thus only tend to coarsen the existing phase separated domains. As an illustration, we plotted on Fig 8 the auto-correlation functions  $g(r)$  of all samples after rescaling  $r/\xi$  both for  $\xi = \xi_{0.5}$  and  $\xi = \xi_{min}$ . As expected in the coarsening stage, we observe that all correlation functions fall onto a master curve, indicating that, regarding the morphology of phase separation, the only changing parameter is a characteristic length scale.

We report on Fig. 9 the time evolution of both correlation lengths  $\xi_{0.5}$  and  $\xi_{min}$  in function of the duration of thermal treatment  $t$  at temperature 650°C. In this plot, we use the cubic root of time for the abscissa in order to reveal the

expected scaling. In these coordinates we get a very good linear behavior over the entire time range experimentally studied (from 1h to 96h). The time evolution of the size of phase separated domains evaluated by AFM thus obeys very well the predicted scaling for coarsening. Extracting the leading coefficients by performing linear fits we obtain  $\gamma D \sim 10^{-18}$  where we took  $v \sim 10^{-29} \text{m}^3$  for a molecular volume. Assuming for the surface tension a value of order  $\gamma \sim 10^{-2} \text{J.m}^{-2}$  this gives us for the value of the interdiffusion coefficient at  $650^\circ$   $D \sim 10^{-16} \text{cm.s}^{-1}$ , which is consistent with literature[12].

### 4.3 Effect of annealing temperature

The same analysis is repeated to analyze the evolution of the correlation lengths  $\xi_{0.5}$  and  $\xi_{min}$  for 16h long heat treatments at temperatures varying from  $625^\circ\text{C}$  to  $680^\circ\text{C}$ . We now test the Arrhenius dependence of the interdiffusion coefficient. The results are reported on Fig 10 in coordinates  $\log \xi$  vs  $1/T$ . We obtain again a reasonable linear behavior indicating that the Arrhenius scaling gives a good approximation of the dependence of the interdiffusion coefficient with temperature.

The values of  $c$  and  $d$  parameters obtained *via* the linear fit  $\ln \xi = c - d/T$  are given in table 3 with their associated standard deviations both for  $\xi = \xi_{0.5}$  and for  $\xi = \xi_{min}$ . Using  $d = E_{in}/3RT$  (the factor 3 coming from the exponent 1/3 in Eq. (3)) we can give a rough estimate of the activation energy  $E_{in} = 135 \pm 45 \text{kJ.mol}^{-1}$ . This value seems to be consistent with typical results from literature: by electrical resistivity measurements in ion exchanged Corning 7740 borosilicate glasses, Garfinkel[27] obtained activation energies in the range  $80 - 120 \text{kJ.mol}^{-1}$ ; activation energies measured for the diffusion of sodium in silicate networks are also in the same range[28].

## 5 Conclusion

Performing selective etching on the surface of phase separated alkali borosilicate glasses, we revealed the phase separated domain by AFM. A quantitative statistical analysis of AFM data allowed us to extract the characteristic correlation lengths of the coarsening stage of phase separation. A systematic study of the dependence on time and temperature of the phase separated domains was performed. We recover the expected cubic root time scaling for the domain size temporal evolution and we could extract an estimate of the interdiffusivity coefficient. The dependence of the latter on temperature is consistent with an Arrhenius behavior, allowing to give a rough estimate of the activation energy for interdiffusion. The numerical values obtained for these two parameters are



moreover consistent with literature data. This study performed on a very simple phase separated glass thus shows that, beyond its performance in imaging, AFM analysis can be used in a more quantitative way to characterize phase separation, and be considered as an alternative or complementary technique to visible or X-ray scattering traditionally used in that purpose.

## Acknowledgement

We benefited from the technical help of A. furet and P. Lambremont for the glass preparation. We thank M.H. Chopinet, P. Garnier, S. Papin, S. Roux and T. Sarlat for useful comments and discussions.

## References

- [1] H. Arribart and D. Abriou. Ten years of atomic force microscopy in glass research. *Ceramics-Silicaty*, 44:121–128, 2000.
- [2] W. Raberg, A.H. Ostadrahimi, T. Kayser, and K. Wandelt. Atomic scale imaging of amorphous silicate glass surfaces by scanning force microscopy. *J. Non-Cryst. Solids*, 351:1089–1096, 2005.
- [3] G.H. Frischat, J.-F. Poggemann, and G. Heide. Nanostructure and atomic structure of glass seen by atomic force microscopy. *J. Non-Cryst. Solids*, 345-346:197–202, 2004.
- [4] P. Daguier, B. Nghiem, E. Bouchaud, and F. Creuzet. Pinning and depinning of crack fronts in heterogeneous materials. *Phys. Rev. Lett.*, 78:1062, 1997.
- [5] T. Sarlat, A. Lelarge, E. Søndergård, and D. Vandembroucq. Frozen capillary waves on glass surfaces: an afm study. *Preprint*, XX:YY–YY, 2006.
- [6] Hwan Kwang Lee Je Young Kim and Sung Chul Kim. Surface structure and phase separation mechanism of polysulfone membranes by atomic force microscopy. *Journal of Membrane Science*, 163(2):159–166, 1999.
- [7] A.N. Zdravkova, J.P.J.M. van der Eerden, and M.M.E. Snel. Phase behaviour in supported mixed monolayers of alkanols, investigated by afm. *Journal of Crystal Growth*, 275(1-2):e1029–e1033, 2005.
- [8] P. Cyganik, A. Budkowski, J. Raczowska, and Z. Postawa. Afm/lfm surface studies of a ternary polymer blend cast on substrates covered by a self-assembled monolayer. *Surface Science*, 507-510:700–706, 2002.
- [9] A. Rasmont, Ph. Leclre, C. Doneux, G. Lambin, J. D. Tong, R. Jrme, J. L. Brdas, and R. Lazzaroni. Microphase separation at the surface of block

- copolymers, as studied with atomic force microscopy. *Colloids and Surfaces B: Biointerfaces*, 19(4):381–395, 2000.
- [10] T. Ichii, T. Fukuma, K. Kobayashi, H. Yamada, and K. Matsushige. Phase-separated alkanethiol self-assembled monolayers investigated by non-contact afm. *Appl. Surf. Sci.*, 210(1-2):99–104, 2003.
- [11] B. Bergues, J. Lekki, A. Budkowski, P. Cyganik, M. Lekka, A. Bernasik, J. Rysz, and Z. Postawa. Phase decomposition in polymer blend films cast on homogeneous substrates modified by self-assembled monolayers. *Vacuum*, 63(1-2):297–305, 2001.
- [12] O.V. Mazurin and E.A. Porai-Koshits, editors. *Phase separation in glass*. North-Holland, Amsterdam, 1984.
- [13] H. Tanaka, T. Yazawa, K. Eguchi, H. Nagasawa, N. Matsuda, and T. Einishi. Precipitation of colloidal silica and pore size distribution in high silica porous glass. *J. Non-Cryt. Solids*, 65(2-3):301–309, 1984.
- [14] S. Polizzi, P. Riello, G. Fagherazzi, and N. F. Borrelli. The microstructure of borosilicate glasses containing elongated and oriented phase-separated crystalline particles. *J. Non-Cryt. Solids*, 232-234:147–154, 1998.
- [15] S. Polizzi, P. Riello, G. Fagherazzi, M. Bark, and N.F. Borrelli. Two-dimensional small-angle x-ray scattering investigation of stretched borosilicate glasses. *Journal-of-Applied-Crystallography*, 30:487–494, 1997.
- [16] M. Tomozawa and T. Takamori. Scattering study of microstructurally birefringent glasses. *J. Am. Ceram. Soc.*, 63(5-6):276–280, 1980.
- [17] S.C. Danforth and J.S. Haggerty. Microstructural characterization of graded-index antireflective films. *J. Am. Ceram. Soc.*, 66(1):C6–C8, 1983.
- [18] T.H. Elmer, M.E. Nordberg, G.B. Carrier, and E.J. Korda. Phase separation in borosilicate glasses as seen by electron microscopy and scanning electron microscopy. *J. Am. Ceram. Soc.*, 53(4):171–175, 1970.
- [19] S. Polizzi, A. Armigliato, P. Riello, N.F. Borrelli, and G. Fagherazzi. Redrawn phase-separated borosilicate glasses: a tem investigation. *Microscopy Microanalysis Microstructure*, 8(3):157–165, 1997.
- [20] Y. Kato, H. Yamazaki, and M. Tomozawa. Detection of phase separation by ftir in a liquid-crystal-display substrate aluminoborosilicate glass. *J. Am. Ceram. Soc.*, 84(9):2111–2116, 2001.
- [21] W.L. Konijnendijk and J.M. Stevels. The structure of borosilicate glasses studied by raman scattering. *J. Non-Cryt. Solids*, 20(2):193–224, 1976.
- [22] W.B. White. Investigation of phase separation by raman spectroscopy. *J. Non-Cryt. Solids*, 49(1-3):321–329, 1982.
- [23] F.A. Sigoli, Y. Kawano, M.R. Davolos, and M.Jr Jafelicci. Phase separation in pyrex glass by hydrothermal treatment: evidence from micro-raman spectroscopy. *J. Non-Cryt. Solids*, 284:49–54, 2001.

- [24] A. Malik, A.R. Sandy, L.B. Lurio, G.B. Stephenson, S.G.J. Mochrie, I. McNulty, and M. Sutton. Coherent x-ray study of fluctuations during domain coarsening. *Phys. Rev. Lett.*, 81:5832–5835, 1998.
- [25] R.W. Balluffi, S.M. Allen, and W.C. Carter, editors. *Kinetics of materials*. Wiley, Hoboken, 2005.
- [26] D.A. Huse. Corrections to late-stage behavior in spinodal decomposition: Lifshitz-slyozov scaling and monte carlo simulations. *Phys. Rev. B*, 34:7845, 1986.
- [27] H.M. Garfinkel. Ion exchange properties of borosilicate glass membranes. *Phys. Chem. Glass.*, 11:151–158, 1970.
- [28] R.H. Doremus. *Glass science*. Wiley-Interscience, New-York, 1973.

<b>Duration</b>	$\xi_{0.5}$ (nm)	$\xi_{min}$ (nm)
1 hour	27	97
4 hours	31	121
8 hours	43	144
16 hours	58	195
32 hours	66	238
64 hours	94	332
96 hours	105	422

Table 1  
Correlation length ( $\xi_{0.5}$  and  $\xi_{min}$ ) *vs* duration of thermal treatment at 650°C.

<b>Temperature</b>	$\xi_{0.5}$ (nm)	$\xi_{min}$ (nm)
625°C	47	148
650°C	58	195
660°C	51	160
670°C	62	191
675°C	63	207
680°C	66	230

Table 2  
Correlation length ( $\xi_{0.5}$  and  $\xi_{min}$ ) *vs* temperature for 16 hours thermal treatment.

$\ln \xi = c - \frac{d}{T}$	c	d
$\xi_{0.5}$	$-11.34 \pm 1.54$	$(4.9 \pm 1.4) \cdot 10^3$
$\xi_{min}$	$-9.43 \pm 2.13$	$(5.6 \pm 1.9) \cdot 10^3$

Table 3  
Parameters from linear curve fitting of  $\ln \xi_{0.5}$  and  $\ln \xi_{min}$  as a function of the inverse of absolute temperatures ( $1/T$ ) for 16 hours thermal treatments.

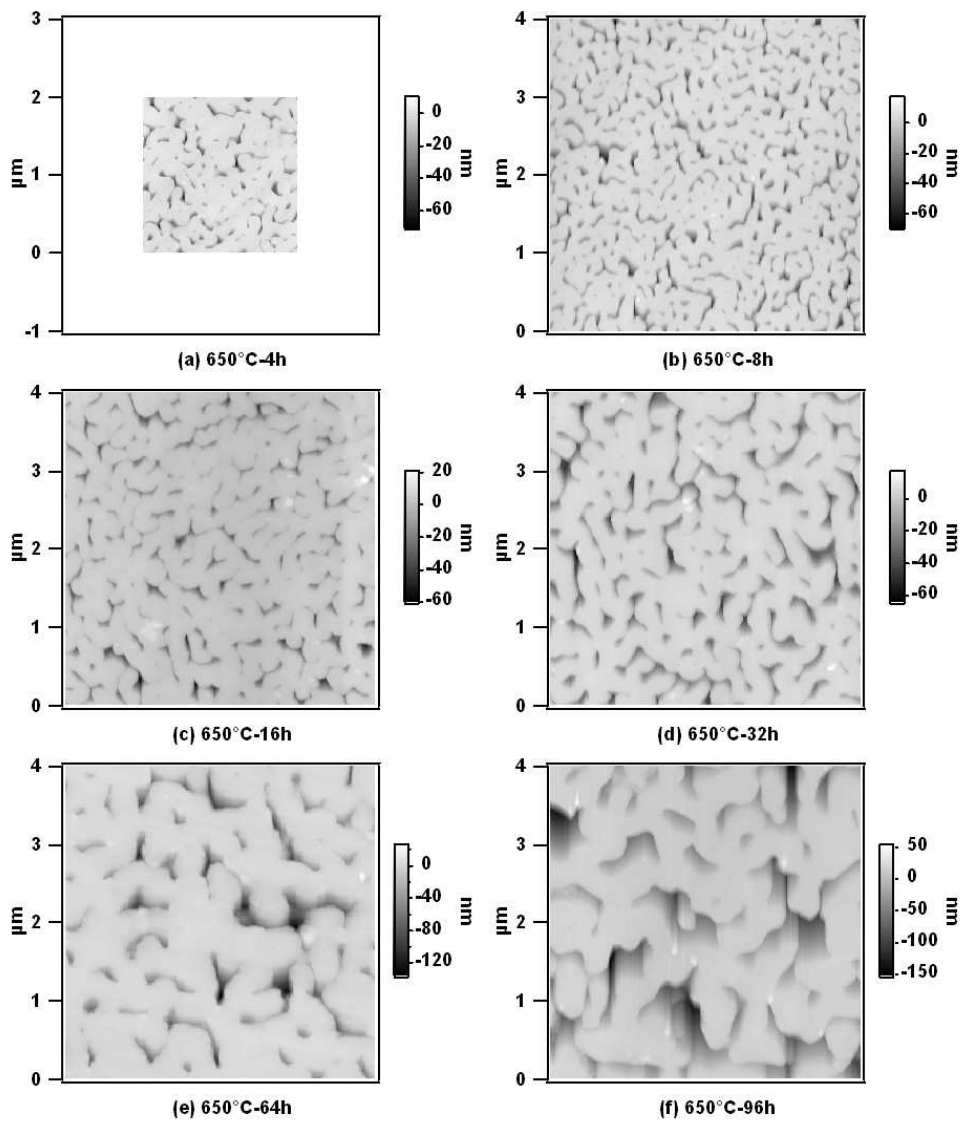


Fig. 1. AFM height images of borosilicate glass samples after thermal treatment at 650°C during six different durations.

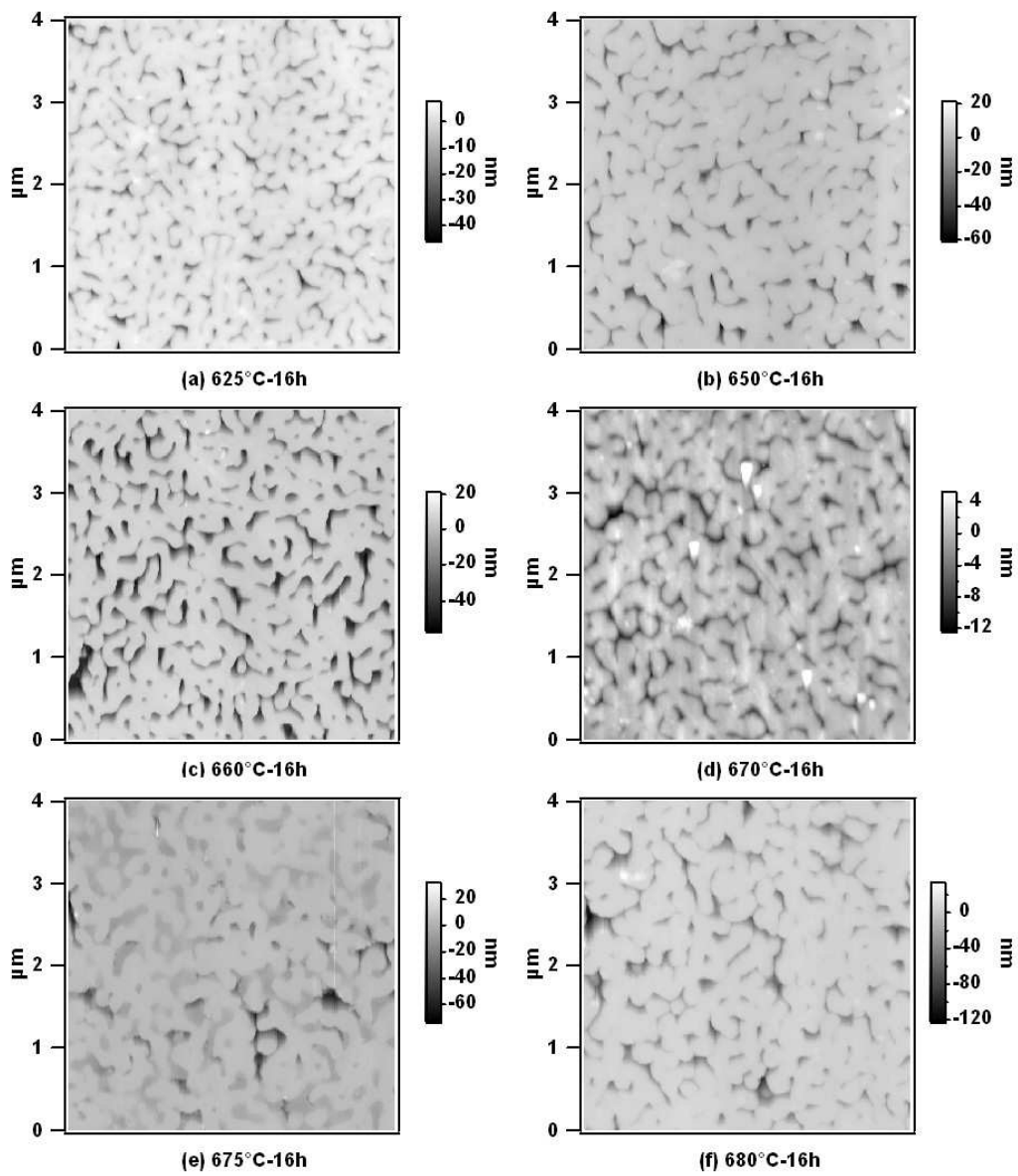


Fig. 2. AFM height images of borosilicate glass samples after 16 hours thermal treatments at six different temperatures.

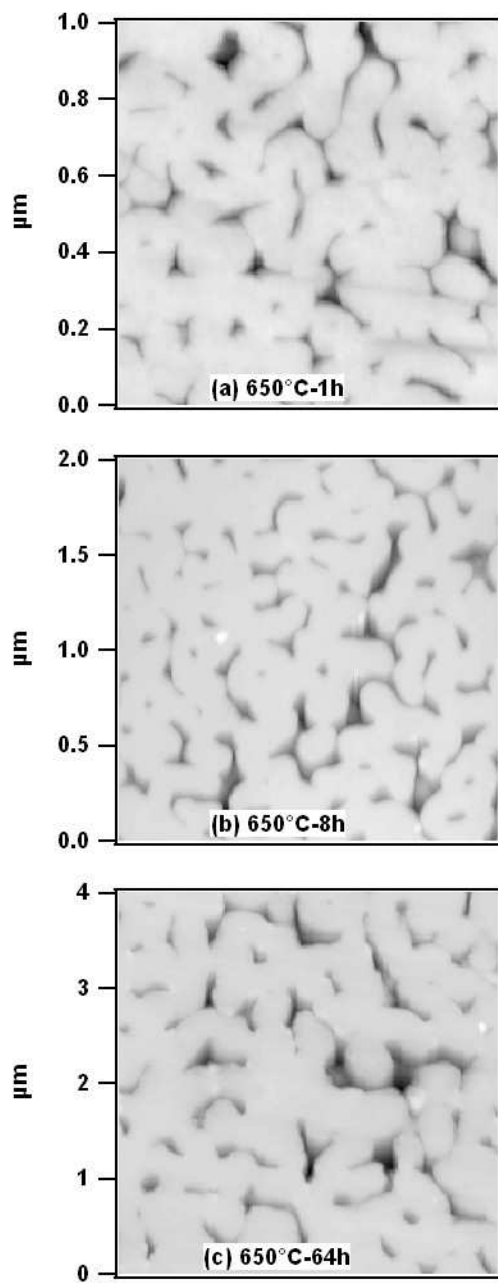


Fig. 3. AFM height images of three borosilicate glass samples. These images illustrate the similarity of morphology of the phase separation domains for various observation scales according to the duration of thermal treatment at  $650^{\circ}\text{C}$ .

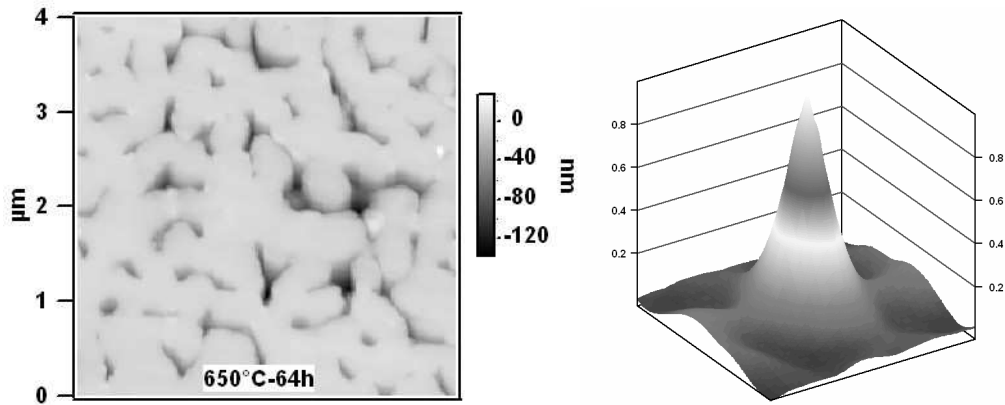


Fig. 4. AFM height images ( $4 \times 4 \mu\text{m}^2$ ) of a borosilicate glass sample after 64 hours of thermal treatment at  $650^\circ\text{C}$  (left) and the associated three dimensional representation of the center part ( $0.5 \times 0.5 \mu\text{m}^2$ ) of the auto-correlation function  $C(\vec{x})$  (right).

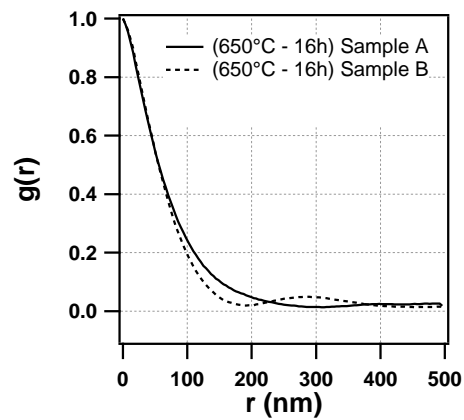


Fig. 5. Radial mean value of the auto-correlation function  $g(r)$  vs distance  $r$  (in nm) for borosilicate glass samples annealed 16 hours at  $650^\circ\text{C}$ . Samples A have been cut and polished after annealing treatment and conversely samples B have been cut and polished before annealing treatment



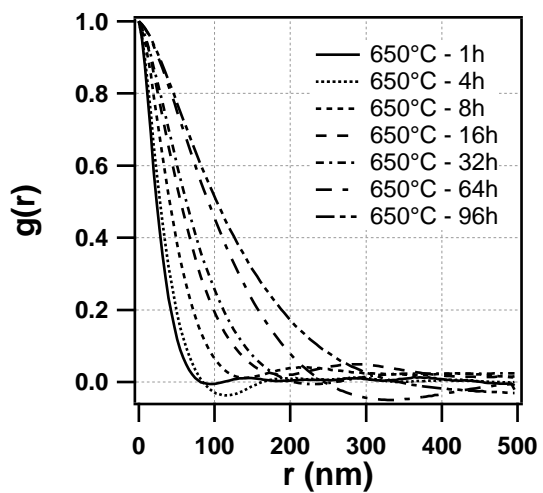


Fig. 6. Radial mean value of the auto-correlation function  $g(r)$  vs distance  $r$  (in nm) for borosilicate glass samples annealed during different durations at 650°C.

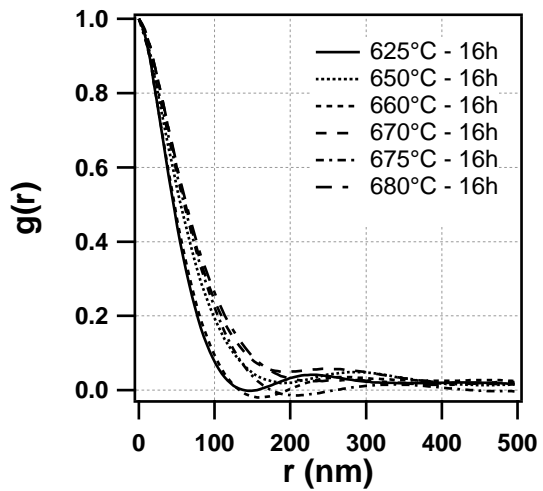


Fig. 7. Radial mean value of the auto-correlation function  $g(r)$  as a function of distance  $r$  (in nm) for borosilicate glass samples annealed during 16h at different temperatures.

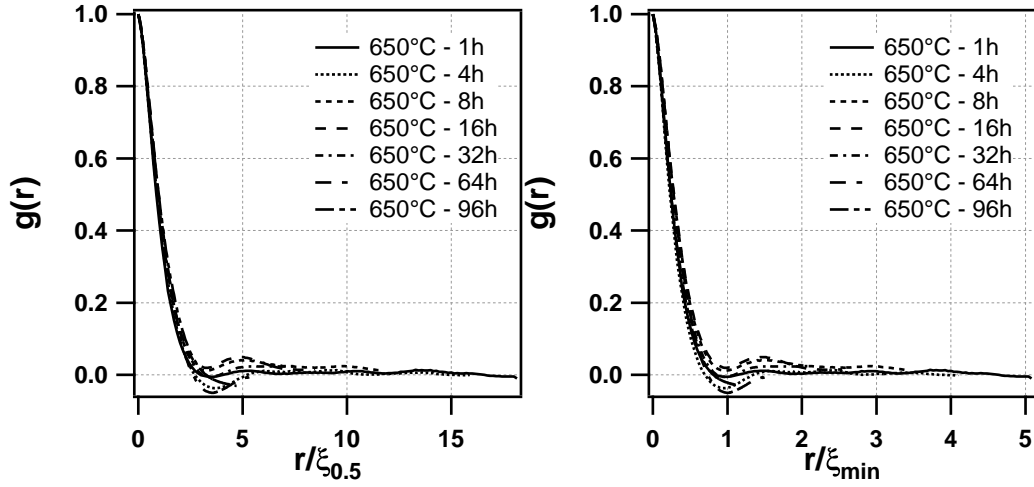


Fig. 8. Radial mean value of the auto-correlation function ( $g(r)$ ) as a function of the normalized distance ( $r/\xi$ ) for borosilicate glass samples after thermal treatment during different durations at  $650^\circ\text{C}$  : (left)  $r$  is normalized with the correlation length  $\xi_{0.5}$  ( $g(\xi_{0.5}) = 0.5$ ) and (right) with the correlation length  $\xi_{min}$  ( $g(\xi_{min}) = \min(g(r))$ ).

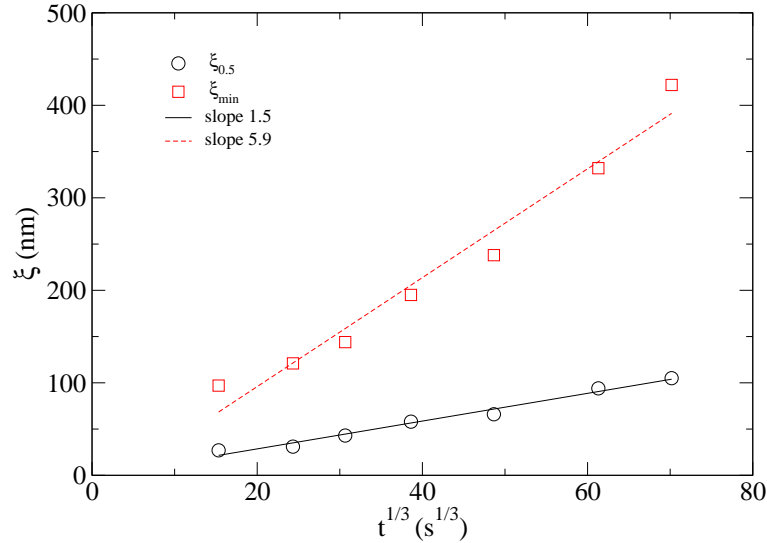


Fig. 9. Evolution of the two correlation length ( $\xi_{0.5}$  and  $\xi_{min}$ ) w.r.t. the duration of thermal treatment at  $650^\circ\text{C}$ .

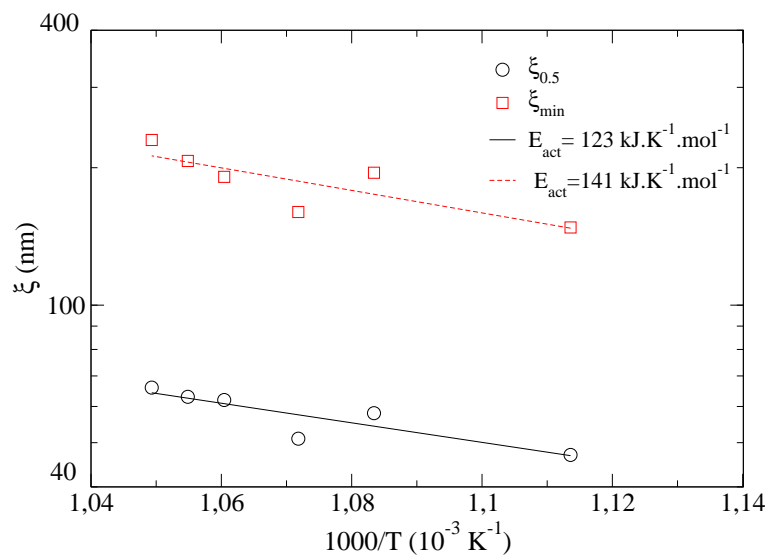


Fig. 10. Evolution of the two correlation lengths ( $\xi_{0.5}$  and  $\xi_{min}$ ) w.r.t. the temperature for 16 hours thermal treatments.